Journal of Petroleum Science and Engineering 178 (2019) 1018–1028

Contents lists available at ScienceDirect

Journal of Petroleum Science and Engineering

journal homepage: www.elsevier.com/locate/petrol

Prediction of permeability and its anisotropy of tight oil reservoir via precise pore-throat tortuosity characterization and "umbrella deconstruction" method

Shuheng Du*

State Key Laboratory of Nonlinear Mechanics, Institute of Mechanics, Chinese Academy of Sciences, Beijing, 100190, China

ARTICLE INFO

Keywords:
Tight oil
Permeability
Pore-throat tortuosity
"Umbrella deconstruction" method

ABSTRACT

This study aimed to investigate the prediction method of permeability and its anisotropy of tight oil reservoir via precise pore-throat tortuosity characterization and "umbrella deconstruction" method combining the approaches of the field emission SEM imaging, high resolution image processing, fine and large-scale mathematical statistics, nonlinear regression and other technical means.

In this paper, the authors proposed the new calculation model of pore-throat tortuosity, the absolute permeability and the permeability anisotropy based on the improved deep understanding of reservoir. Results of the prediction on the tight oil reservoir of "YANCHANG" formation in Ordos Basin show that the errors of the new method in this paper are the smallest among the total five methods, respectively $0.023 \times 10^{-3}\mu m^2$ and $0.090 \times 10^{-3}\mu m^2$; the average values of other four methods were $0.090 \times 10^{-3}\mu m^2$ and $0.108 \times 10^{-3}\mu m^2$, respectively. The predicted results have higher accordance with the measured results, which proved the practicality of the new method. The samples has the highest permeability at the angle of 0°(180°/360°) and the permeability values are equal to $0.25 \times 10^{-3}\mu m^2$. Similarly, the sample has the lowest permeability at the angle of 22.5°(202.5°), 90°(270°), and 112.5°(292.5°), the permeability values are all equal to $0.06 \times 10^{-3}\mu m^2$. At the same time, the calculation of permeability anisotropy results shows that the anisotropy of tight oil reservoirs is very significant, and the permeability value in one direction is obviously higher than which in other directions.

It is concluded that the precise description of pore throat geometry, especially the calculation of pore-throat tortuosity parameter, is one of the most important parameters affecting the prediction accuracy of permeability theoretically. Meanwhile, there are dominant seepage channels, which would play a very important guiding role in the prediction of hydrocarbon accumulation and seepage capacity.

The conclusion will provide a more rigorous theoretical basis for the rapid and accurate evaluation of the physical properties of unconventional reservoirs.

1. Introduction

Permeability, as an important parameter for evaluating the physical properties of the reservoir, largely reflects reservoir productivity level. According to the parameter of permeability, three major heterogeneities, i.e. surface heterogeneities, interlayer heterogeneities and intra-layer heterogeneities, can be derived, and the differences of reservoir and seepage levels can be described from a macro perspective, so as to achieve the goal of comprehensive evaluation of reservoir quality.

As to the permeability prediction, it was found that Beckingham et al. (2013) and other researchers compared the predicted and measured permeability values based on SEM. It was believed that the distortion of surface roughness into pore throat resulted in the underestimation of permeability. Arash et al. (2016) estimated three-dimensional coordination numbers from two-dimensional cross-sectional images and explored the error of absolute permeability prediction using pore network flow model. An et al. (2016) studied the effects of pore throat ratio, coordination number and pore throat orientation on absolute permeability using a regular network model. Shah et al. (2016) predicted the properties of pore network, such as the number of pore and throat, average pore throat radius and coordination number, and used Lattice Boltzmann (LBM) or pore network (PNM) modeling to simulate single-phase and dual-phase flow. Three-dimensional core image can be obtained after CT scanning, and digital core can be built after filtering and segmentation. Yang et al. (2016) gets the rock

* Corresponding author.
E-mail address: dushuheng@imech.ac.cn.

https://doi.org/10.1016/j.petrol.2019.03.009
Received 15 December 2018; Received in revised form 16 February 2019; Accepted 3 March 2019
Available online 09 March 2019
0920-4105/

structure characteristics by analyzing the Geometry-Topology structure of the extracted pore network model, and carries out sandstone flow analysis through numerical simulation. Patrick et al. (2017) established a porosity index and pore resistivity model to explore the permeability of carbonate rocks in northeastern Brazil. Nishank et al. (2017a, b) comprehensively assessed the differences in the solution of seepage solvers including Lattice-Boltzmann, computational fluid dynamics, voxel-based, fast semi-analysis and known empirical models. It was concluded that the main causes of the errors included parameterization of basic physical equations, differences in boundary conditions and numerical convergence criteria. The parameterization of physical equation needs further optimization. Nishank et al. (2017a, b) also studied the error of image segmentation threshold and image voxel size in calculating image permeability, and proposed a correction method between laboratory measured values and digital rock calculated values. Arash et al. (2017) respectively predicted permeability based on neural network model and empirical equation with both porosity and average coordination number, but they could not explain carbonate permeability well. Song et al. (2018) considered the size distribution combination of organic and inorganic pore, studied its influence on gas flow by numerical simulation. Kirill et al. (2018) proposed the Stokes solver (FDMSS) for three-dimensional pore geometry, which directly studies pore fluid flow simulation and permeability assessment in three-dimensional voxelized pore geometry (i.e. meshless). All the above studies show that the micro-details of reservoirs have a great impact on the theoretical prediction of permeability. In other words, the accurate description of pore throat geometry is an indispensable part of improving the accuracy of permeability prediction.

Pore-throat tortuosity is the ratio of the actual length of the seepage channels and the apparent length the fluids flow through the seepage medium (the macro distance). Fluid particles flow through the medium in unit distance—the actual length of motion trajectory of the particle; this is an important parameter for the evaluation of the complexity of the seepage channel, but also one of the most important parameters in the prediction of reservoir permeability (Lonnes et al., 2003; London et al., 2014; Arash et al., 2014; Huang and Zhao, 2017; Nishank et al. (2017a, b)).

As to the pore-throat tortuosity calculation, in the early studies, the pore-throat tortuosity was measured directly by the casting sheet, but measurement efficiency was low and accuracy was limited. In recent years, scholars have carried out a great deal of research in related fields in order to increase both the accuracy and the efficiency of such measurements. Plessis and Masliyah (1988) investigated the relationship between pore-throat tortuosity and porosity. Sen et al. (1981), Boundreau et al. (1996), Comiti et al. (2000), and other scholars tried to solve this problem based on the experimental summary. Koponen et al. (1996) used the LG numerical simulation to give the expressions of pore throat curvature and porosity in porous media, respectively. Lv et al. (2000) proposed gas permeability method. Yu et al. (2016) calculated the average pore-throat tortuosity by porosity based on the model of curved pipe while. Chen et al. (2011) gave an empirical equation of pore-throat tortuosity. In that equation, the tortuosity is only the function of porosity, and the form is relatively simple, but whether it is robust enough to characterize the factors of pore-throat tortuosity accurately is still questionable. However, the above estimation methods have many shortcomings: Among other issues, they include too many estimation parameters, are difficult to obtain, and the estimation mechanisms tend to be too complex.

Based on a great deal of literature research and analysis, the author thinks that the pore-throat tortuosity results measured by different methods are quite different from each other and are relatively poor in comparison; this makes the physical meaning unknown and it is difficult to verify the accuracy each of these methods when compared to the others. For example, with a capillary force test and seepage test, the randomness of sampling direction and the random starting position of the flow could have randomized the seepage results, so the test results of a single sample or a low number of samples represent only a single or a small number of pores and throats through which the fluid flows, but it cannot accurately and consistently reflect the overall features of reservoir space. In addition, due to the brevity of the seepage test, the unreliability of the experimental results is further exaggerated. This is somewhat similar to the limitations of the high-pressure mercury pressure test. Similarly, pore-throat tortuosity measurement methods of image processing are mostly concentrated in the manual measurement based on the cast slice images under the polarizing microscope. It may cause the lack of automation program, and the measurement process has built into it a certain randomness, so the limitation is obvious: A simplified estimation model of the pore-throat is too idealistic, so the accuracy of the calculated result is worth considering (Piela et al., 2009; Peng et al., 2011; Rajkumar et al., 2012; Beckingham et al., 2013; Ren et al., 2015; Kenneth et al., 2018).

As is obvious in the above research, most of the pore-throat tortuosity estimation methods focus on experimental testing and simplified modeling, and the majority of experimental and numerical simulation methods treat the reservoir with high porosity and medium permeability as the research object. Thus, the numerical simulation of the Koponen method could be used only for a reservoir exhibiting a porosity higher than 33%. Results of the other studies could only be used for a reservoir with a porosity higher than 15%. For the tight sandstone reservoir, more effective estimation methods were still lacking. Is the pore-throat tortuosity of the tight sandstone reservoir only controlled by the single factor of porosity? This has also not been reported in the literature. In addition, accurate estimation methods based on the concept of the original pore-throat tortuosity are still few, the reservoir pore-throat tortuosity estimation methods used are still not stringent and their results remain unclear (Rhiannon et al., 2016; Shah et al., 2016; Rikan et al., 2017; Song et al., 2017; Yang et al., 2017).

Based on these limitations, a new pore-throat tortuosity estimation method is proposed so the new permeability prediction model is also proposed in this paper.

In addition, the anisotropy of reservoir permeability is also an important issue of great concern in petroleum geology and engineering. If we want to predict the anisotropy of permeability, we must firstly understand the development of pore throats and minerals in all directions of reservoir, and the conclusion should be representative, that is to say, the observation scale should not be too small. “Umbrella deconstruction” technology is a new technology proposed by Du et al., in 2018 to accurately characterize the heterogeneity and anisotropy of pore throats and minerals in unconventional oil and gas reservoirs on a large horizon scale. This method takes the lead in alleviating the contradiction between resolution and observation scale of unconventional reservoir in two-dimensional space. This paper intends to combine this method to study the heterogeneity of reservoir permeability.

In this paper, we followed the original characteristics of the reservoir, then closely focused on characteristics such as pore size, structure and so on. In accordance with our goal of accurately describing the pore and throat in the full range, we calculated the pore-throat tortuosity of the unconventional reservoir under the multi-scale, and applied the tortuosity values to the fast prediction of matrix permeability in an unconventional sandstone reservoir in Ordos Basin, China, using the extension form of Kozeny-Carman equation. At the same time, “umbrella deconstruction” was carried out for tight oil reservoirs, and quantitative prediction of permeability anisotropy of tight oil reservoirs was also carried out in combination with the new pore-throat tortuosity calculation method and permeability prediction model proposed in this paper.

2. Geologic setting

The Ordos Basin is located in the western part of the north China landmass (Fig. 1). It is a large multicycle craton basin with the occurrence of whole lift and depression migration, and the structure inside

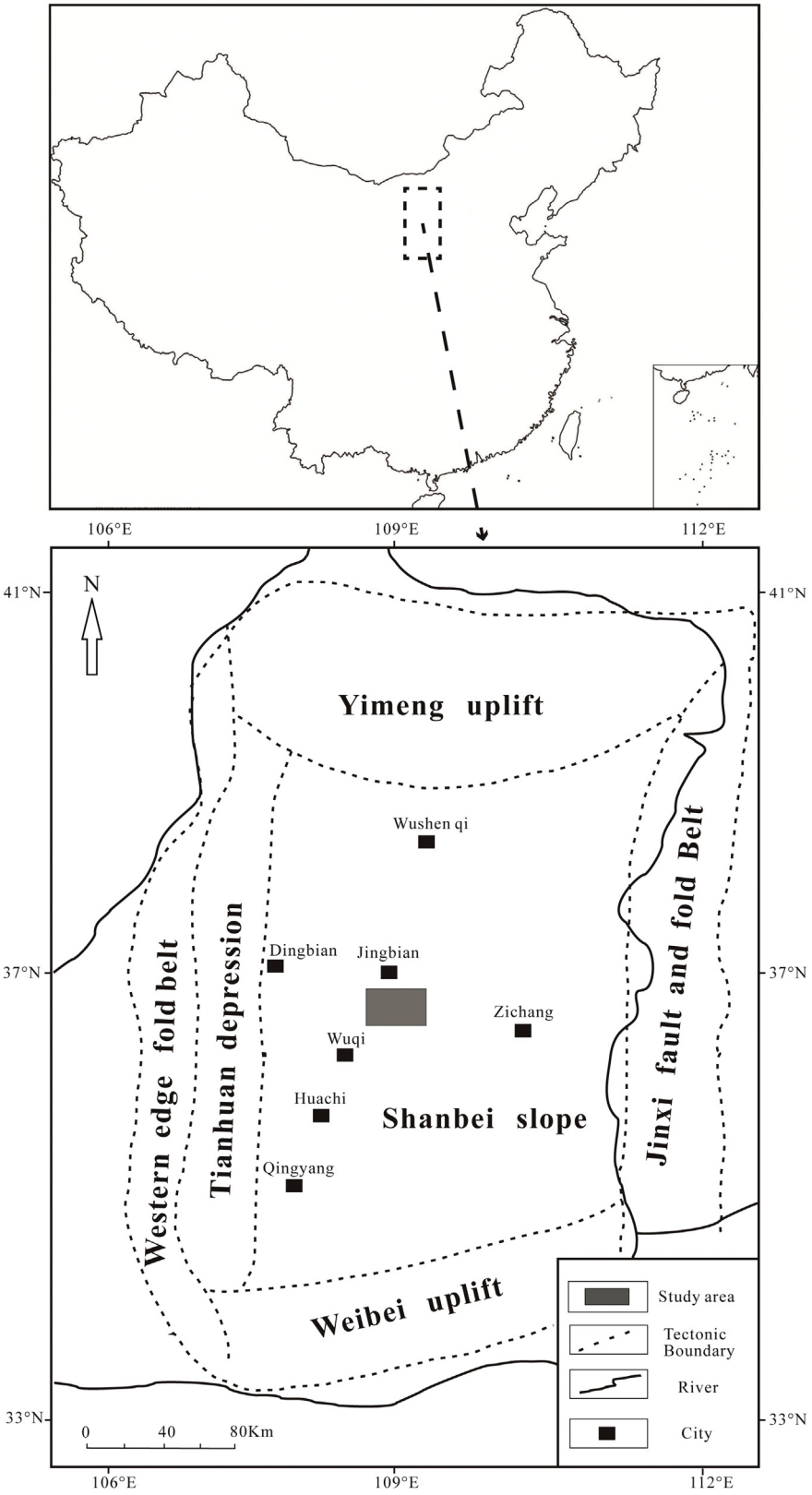

Fig. 1. Location of study area in Ordos Basin, China (Du et al., 2019).

the basin is relatively simple. Abundant oil resources existed in the Upper Triassic the ultra-low permeability Yanchang Formation, which is part of a lake-delta sedimentary system (Du et al., 2018a and 2018b).

The study area is located in the southwestern part of the northern Shanxi slope in the Ordos Basin. The "YANCHANG" formation belongs to the clastic rock dominated by lacustrine sediments in Late Triassic. The physical properties are poor, the average porosity is 8.85%, and the permeability is $0.16 \times 10^{-3}\mu m^2$. The pore types are mainly inter-granular pore and dissolved pore; the primary inter-granular pore, secondary inter-granular pore and secondary dissolved pore are

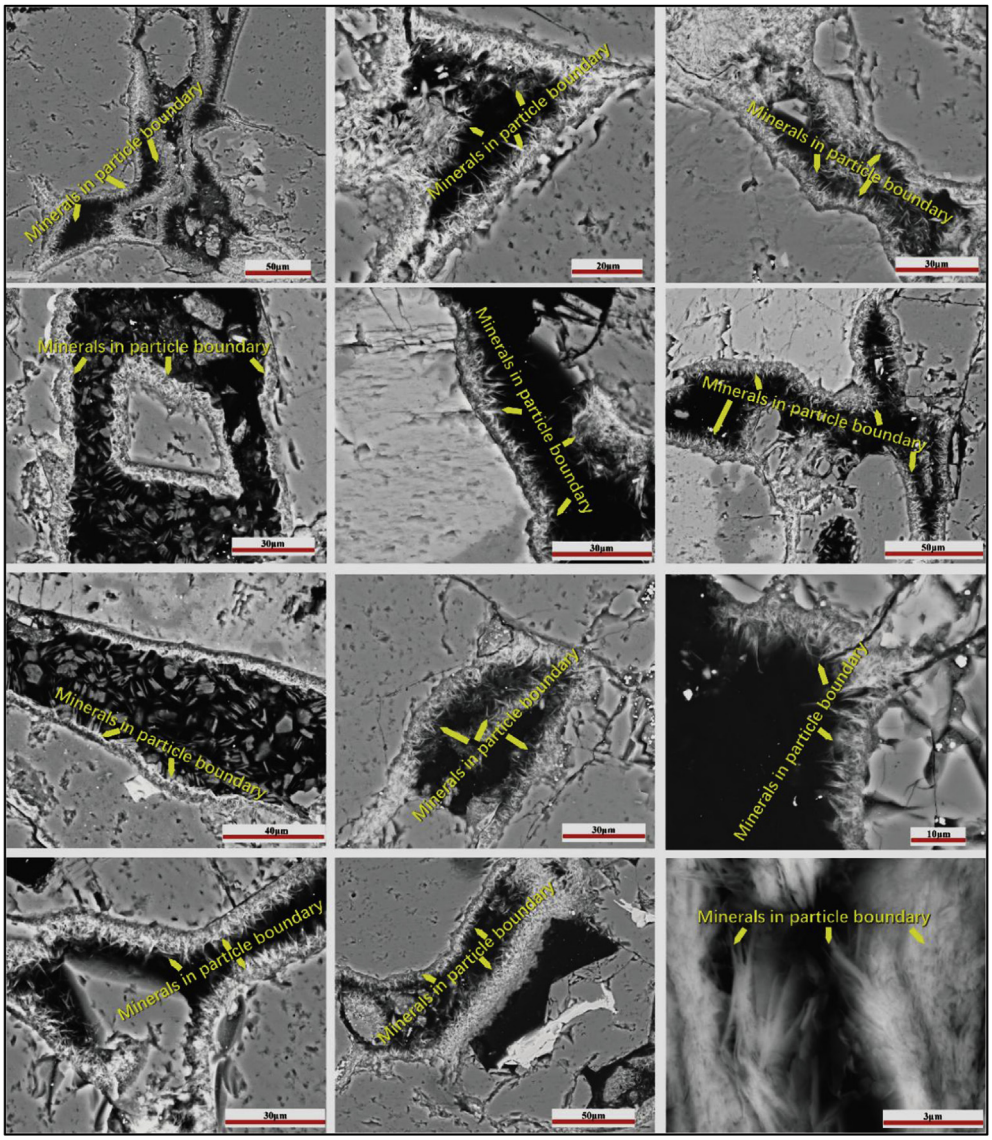

Fig. 2. SEM observation of the minerals in the particle boundary in an unconventional reservoir.

relatively developed (Xiong et al., 2016).

3. Methods and principles

3.1. Methods development of permeability prediction

First of all, it is necessary to point out that understanding the fluid flow in porous media, especially the micro-nano pore-throat, is an extremely complex issue. The influencing factors focused mainly on three aspects: the fluid properties (Newtonian or non-Newtonian), pore-throat characteristics (size, direction, tortuosity and mineral types in the pore-throat boundary), and interaction between fluid and minerals in the particle boundary (physical adsorption, chemical corrosion and so on) (Fig. 2).

Therefore, the macro distance of the fluid motion can be easily determined, but the actual streamline is far more complex than the macro trajectory; such things as the fluid reflux could make measurement difficult. When we use the "pore-throat divide-union" method to calculate the pore-throat tortuosity, the fluid reflux is fully considered in the equation. When we compared development characteristics of the pore-throat with those of the river channels in the later periods (such as a meandering river and a braided river), we saw that the bending outer boundary of the pore-throat would cause the streamline dispersion and fluid reflux should be carefully observed. Therefore, after full consideration of the diversity and complexity of pore-throat distribution and the real streamlines, we use the "n" times of pore-throat perimeter ("n" is determined by the actual flow process and it could be any positive value) to indicate the actual flow distance of the fluid flow-through, which can greatly highlight the diversity and energy consumption in the process of seepage, and is thus more practical.

Kozeny (1927) and Carman (1939) proposed Kozeny-Carman equation (KC equation) based on capillary bundle model, namely:

$$K = \frac{\varphi^3}{CS^2} \tag{1}$$

In equation (1), "K" indicates the permeability, the unit is "$10^{-3}\mu m^2$"; "φ" indicates the porosity, the unit is "%"; "S" indicates the surface area, the unit is "m^2"; "C" indicates the KC constant, which is generally considered to be related to pore-throat tortuosity. KC equation could obtain the pore and permeability parameters in spatial sense based on the infinitesimal element volume analysis method, which solves the problem of theoretical prediction of permeability to a certain extent. Researchers have found that the KC constant is closely related to the micro-pore structure of porous media, so many methods have been

used to modify the KC equation. However, this does not mean that all the problems on theoretical prediction of permeability have be solved. When we use equation (1) to calculate permeability, the acquisition of KC constant is still an important bottleneck problem, but there is still no good calculation method for this KC constant related to pore-throat tortuosity at present, which leads to the theoretical prediction accuracy of permeability still has room for improvement.

In order to predict permeability more conveniently and quickly, Li and Zhang (2007) gave a simplified generalization of KC equation according to the unified model of pipe flow and seepage flow which is:

$$K = \frac{\varphi r^2}{8\tau} \tag{2}$$

In equation (2), "φ" indicates the porosity, the unit is "%"; "r" indicates the pore radius, the unit is "μm", "τ" indicates the pore-throat solidity.

Taking equation (2) as an example, we can think about the problem that if we get the exact value of each parameter in this equation, then the permeability can be calculated accurately to a large extent. Equation (2) involves three variables, the porosity (φ), the radius of capillaries (r) and the pore-throat tortuosity (τ). As to the reservoir sample, if the pore throat structure is obtained by high precision imaging technology, the porosity (φ), and the radius (r) of capillaries were all easily obtained parameters. However, many methods could obtain the pore-throat tortuosity but the accuracy is difficult to control so it needs to be studied emphatically.

In a word, the accuracy of permeability prediction depends on the accuracy of pore-throat tortuosity parameters.

3.2. Assumptions of the new method

The assumptions of the new method is mainly based on the establishment of a new theoretical model of pore throat and the new understanding of the original definition of pore -throat tortuosity. SEM observation on the unconventional reservoir shows (Fig. 2) that the minerals in the particle boundary could be widely found under the microscope. In order to figure out the mineral type, element analysis on the minerals in the particle boundary has also been done (Table 1). The result of that analysis shows that illite plays the most important role in the particle boundary. With the growth of these minerals in an unconventional reservoir, the shape of the pore-throat could become more complex. The significance of these minerals, which grow in the particle boundary in the fluids' seepage process, should never be ignored. We should pay much more attention to this point when we investigate the precise method of permeability estimation of the unconventional reservoir.

Table 1
Element analysis on the minerals in the particle boundary in an unconventional reservoir.

Elements\Sample number	1	2	3	4	5
C	29.64%	70.77%	29.08%	32.58%	10.59%
Na	0.14%	0	0	0	0
Mg	0.11%	0.53%	2.63%	0.42%	5.77%
Al	1.03%	2.06%	6.03%	4.82%	5.23%
Si	1.82%	2.52%	8.27%	7.20%	9.25%
K	0	0	0.28%	1.41%	1.55%
Fe	1.27%	1.76%	2.11%	0	3.74%
O	65.93%	22.26%	51.60%	53.35%	58.52%
F	0	0	0	0	5.00%
Ti	0	0	0	0	0.35%
Cl	0.06%	0.10%	0	0.22%	0
Mineral Type	Illite				

3.3. Solutions of the new method

Fig. 3 is the diagrammatic sketch of single pore-throat tortuosity estimation after considering the minerals in the particle boundary. According to the seepage theory, the fluid would flow through all connected pore-throats when the fluid flows in every direction and the percolation process continues for a long enough time.

The estimation method is as follows. First, we calculated the perimeter of single pore-throat (boundary length of a single pore-throat), and the average perimeter of all the pore-throats that could be obtained. Then, in order to obtain the apparent length (i.e., the macroscopic distance) of the fluid flowing through, we set up the related program, and conducted the Legendre ellipse fitting for the single pore-throat, generating the average long axis length of the Legendre ellipse of all pore-throats. Finally, according to the definition of pore tortuosity, when fluid flows through the pore-throat, the pore-throat tortuosity is the ratio of n times the average pore throat perimeter and the average the major axis length of the Legendre ellipse.

The concrete equation is as follows:

$$\bar{\tau} = \frac{n\bar{P}}{\overline{L_a}} \tag{3}$$

In equation (3), "$\bar{P}$" indicates the average perimeter, the unit is μm; "n" indicates constants Ce with the original properties of reservoir, dimensionless; "$\overline{L_a}$" indicates the average length of major axis of the Legendre ellipse, dimensionless.

The equation (3) is the estimation equation of single pore-throat tortuosity. Because the whole reservoir consists of thousands of pore-throats, the parameters in the above equation are all the average values, so the final result is the average pore-throat tortuosity.

3.4. Prediction of permeability with high efficiency

Taking the SEM and CT images of the tight sandstone reservoir as the original data, image processing should be carried out (Fig. 4). First we use the inter-modes algorithm to calculate the threshold of each image (Fig. 4-(1)). Second, we extract the pore-throat (Fig. 4-(2)). Third, a discrete single pore-throat is taken to calculate the tortuosity of the single pore-throat. (This step indicates the "divide" in the "pore-throat divide-union.") Last, we calculate the average value of all the pore-throats, treating this value as the final tortuosity of the reservoir. (This step indicates the "union" in "pore-throat divide-union.")

The equation (2) shows that the pore-throat tortuosity (τ) is a rather important unknown parameter in the KC equation used to calculate the permeability. Therefore, the reasonable estimation of the pore-throat tortuosity, combined with the statistical estimation of the pore-throat parameters, can be effectively applied to the prediction of the reservoir permeability. When we put equation (3) into (2), we get the final equation of permeability estimation (Equation (4)).

$$\bar{K} = \frac{\varphi \bar{r}^2 \bar{L}_a^2}{8n^2\bar{P}^2} \tag{4}$$

In equation (4), "$\bar{r}$" indicates the average pore-throat radius, the unit is μm.

3.4.1. Permeability anisotropy determination when combing "umbrella deconstruction" method

The steps of the "umbrella deconstruction" method" are like followings (Fig. 5). First, we drilled the standard core sample of the tight oil reservoir. Second, we draw 8 remarkable lines every 22.5° in the overlook surface of the sample. Third, we cut the thin sections along the 8 lines. Fourth, we use the FE-SEM instrument to characterize the reservoir in 8 thin sections and get the images with high resolution. Fifth, we use the new and more precise theoretical model to predict the permeability of 8 thin sections. Finally we could draw the curve of the permeability changing with angels and evaluate the microscopic

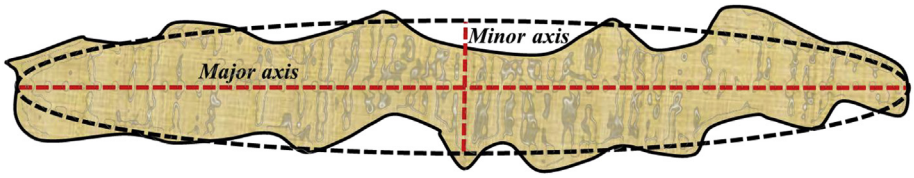

Fig. 3. Diagrammatic sketch of single pore-throat tortuosity estimation after considering the minerals in particle boundary.

heterogeneity of the permeability potential in tight oil reservoir.

3.5. Simplified form of the new permeability prediction model

In order to predict the permeability more rapidly and increase the applicability of the new model, we need to discover the simplified form of the new permeability prediction model proposed in this study which means that as long as we get some general parameters like porosity of the reservoir, we could get the precise value of its permeability.

In order to achieve the above goal, we combined field emission SEM imaging, the pore throat theory model, high resolution image processing, fine large-scale mathematical statistics, nonlinear regression and other technical means to predict the permeability of the unconventional sandstone reservoir of the "YANCHANG" formation in the Xin'anbian area, Ordos Basin, China. Results showed that the predicted results have a higher accordance with the measured results, which proved the practicality of the new method. This approach will provide a more rigorous theoretical basis for the rapid and accurate evaluation of the physical properties of tight reservoirs.

We also applied four other methods proposed by domestic and foreign scholars in carrying out the pore-throat tortuosity estimation; thus we could generate five kinds of pore-throat tortuosity values. Combined with the Kozeny-Carman equation, the reservoir permeability could be predicted and five kinds of permeability values could be obtained. Then, correlation analysis between porosity and five types of permeability prediction values was carried out and five types of relationships between porosity and permeability could be obtained. Finally, the permeability could be predicted by combining the measured porosity with five types of relations between porosity and permeability, and comparison among the five prediction results and the measured permeability was performed to verify the applicability and accuracy of the new method.

Table 2 shows that, as to the unconventional sandstone reservoir "YANCHANG" formation in the Xin'anbian area, the porosity is concentrated between 1.799% ~ 4.833%, and the average value is 3.605%; the average radius of pore-throat is 5.847 μm–8.180 μm, while the average value is 7.399 μm; the average perimeter of pore-throat in 32.631 μm–48.325 μm, and the average value is 42.555 μm; the average length of long axis of pore-throat is 7.501 μm–10.698 μm, and the average value is 9.634 μm.

We will compare the calculation results with those of the other four theoretical methods for calculating the pore-throat tortuosity. The computational equations of the four methods are as follows (equations (5)–(8)):

$$\tau(\mathrm{Yu}) = \frac{1}{2}\left[1 + \frac{1}{2\sqrt{1-\varphi}} + \sqrt{1-\varphi}\,\frac{\sqrt{\left(\frac{1}{\sqrt{1-\varphi}} - 1\right)^2 + \frac{1}{4}}}{1-\sqrt{1-\varphi}}\right] \tag{5}$$

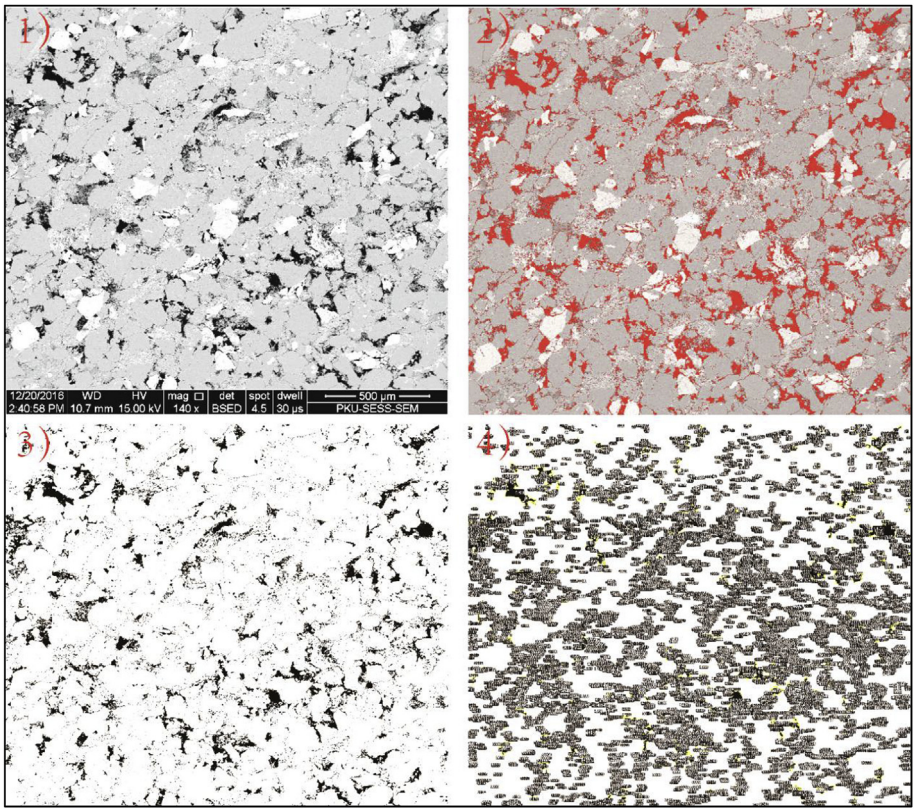

Fig. 4. Image processing process of "YANCHANG" tight sandstone reservoir.
Note: (1) source image; (2) threshold estimation; (3) pore-throat extraction; (4) parameter estimation.

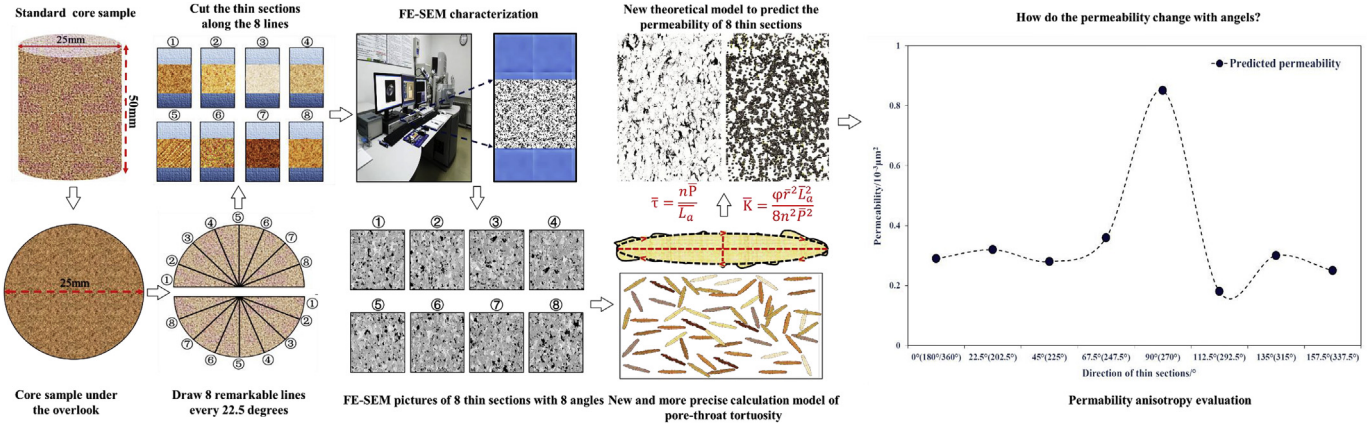

Fig. 5. Comprehensive technical process of the permeability prediction and its anisotropy in tight oil reservoir of yanchang formation in ordos basin via "umbrella deconstruction" method and precise pore geometry characterization.
(Modified from Du et al., 2018a and 2018b).

Table 2
Test and statistics of the pore-throat parameters of the unconventional sandstone reservoir "YANCHANG" formation in Xin'anbian area, Ordos Basin, China.

Sample number	Porosity/%	Average radius of pore-throat/μm	Average perimeter of pore-throat/μm	Average semi long-axis of pore-throat/μm
A83-1	4.284	7.720	43.631	9.937
A83-2	2.464	6.724	37.920	8.632
A83-3	2.528	6.891	37.923	8.756
A83-4	4.601	7.891	44.865	10.237
A83-5	3.700	7.282	42.766	9.551
A83-6	4.602	7.927	44.741	10.211
A83-7	2.219	6.526	35.854	8.351
A83-8	1.799	5.847	32.631	7.501
A83-9	4.218	7.572	42.029	9.756
A83-10	4.205	7.452	44.292	9.913
A83-11	4.833	8.180	48.325	10.698
A83-12	2.578	6.984	40.580	8.993
A83-13	3.379	7.397	40.190	9.604
A83-14	3.836	7.476	42.971	9.747
A83-15	3.560	7.320	42.909	9.690
A83-16	3.206	7.451	42.942	9.582
A83-17	3.977	7.434	42.489	9.678
A83-18	3.355	7.394	40.814	9.516
A83-19	3.683	7.244	43.113	9.606
A83-20	4.505	7.802	45.522	10.302
A83-21	3.115	7.430	41.088	9.588
A83-22	3.789	7.424	41.569	9.564
A83-23	3.355	7.114	41.193	9.435
A83-24	3.394	7.163	42.964	9.426
A83-25	4.167	7.602	45.967	10.064
A83-26	3.783	7.823	44.241	10.116
A83-27	4.000	7.794	46.321	10.232
A83-28	3.493	7.202	42.102	9.472
A83-29	2.931	7.064	41.522	9.195
A83-30	4.105	7.676	44.077	10.005
A83-31	4.033	7.822	44.369	10.225
A83-32	3.670	7.672	45.949	10.093
A83-33	3.476	7.216	42.558	9.507
A83-34	3.166	7.562	42.591	9.731
A83-35	4.176	7.895	46.409	10.265

$$\tau(\text{Chen}) = \varphi^{-\frac{3}{4}} - 0.35 \quad (6)$$

$$\tau(\text{Koponen}) = 0.8(1-\varphi) + 1 \quad (7)$$

$$\tau(\text{Plessis}) = 1 + \sqrt{1-\varphi} \quad (8)$$

In equations (5)–(8), "φ" indicates the porosity. As can be seen in Table 3, there are obvious differences in the pore-throat tortuosity values calculated by the five methods, so there will also be differences in the applicability and prediction accuracy of the five methods. The sequence of the average pore-throat tortuosity values of all samples calculated by five methods is τ(Yu) > τ(Chen) > τ(This study) > τ(Plessis) > τ(Koponen). We can see that the value predicted by the new method falls in the center of the values predicted by the five methods, so it is thus possible to make a relatively objective prediction of permeability.

It needs to be pointed out that in the estimation process, "n" in equation (3) was set from 0 to 1000 (in increments of 0.5). Practice

Table 3
Test and statistics of pore-throat tortuosity of the unconventional sandstone reservoir "YANCHANG" formation in the Xin'anbian area, Ordos Basin, China (five methods).

Sample number	τ(This study)	τ(Yu & Li)	τ(Chen)	τ(Koponen)	τ(Plessis)
A83-1	2.195	12.062	10.270	1.766	1.978
A83-2	2.197	20.676	15.729	1.780	1.988
A83-3	2.165	20.162	15.423	1.780	1.987
A83-4	2.191	11.259	9.716	1.763	1.977
A83-5	2.239	13.902	11.504	1.770	1.981
A83-6	2.191	11.256	9.714	1.763	1.977
A83-7	2.147	22.915	17.043	1.782	1.989
A83-8	2.175	28.174	20.008	1.786	1.991
A83-9	2.154	12.244	10.394	1.766	1.979
A83-10	2.234	12.281	10.419	1.766	1.979
A83-11	2.259	10.738	9.351	1.761	1.976
A83-12	2.256	19.779	15.193	1.779	1.987
A83-13	2.092	15.184	12.338	1.773	1.983
A83-14	2.204	13.423	11.187	1.769	1.981
A83-15	2.214	14.433	11.851	1.772	1.982
A83-16	2.241	15.982	12.849	1.774	1.984
A83-17	2.195	12.961	10.879	1.768	1.980
A83-18	2.144	15.290	12.406	1.773	1.983
A83-19	2.244	13.964	11.545	1.771	1.981
A83-20	2.209	11.490	9.877	1.764	1.977
A83-21	2.143	16.437	13.137	1.775	1.984
A83-22	2.173	13.585	11.294	1.770	1.981
A83-23	2.183	15.290	12.406	1.773	1.983
A83-24	2.279	15.119	12.296	1.773	1.983
A83-25	2.284	12.389	10.493	1.767	1.979
A83-26	2.187	13.605	11.308	1.770	1.981
A83-27	2.264	12.889	10.830	1.768	1.980
A83-28	2.222	14.702	12.027	1.772	1.982
A83-29	2.258	17.444	13.767	1.777	1.985
A83-30	2.203	12.570	10.615	1.767	1.979
A83-31	2.170	12.787	10.762	1.768	1.980
A83-32	2.276	14.012	11.576	1.771	1.981
A83-33	2.238	14.772	12.072	1.772	1.982
A83-34	2.189	16.179	12.973	1.775	1.984
A83-35	2.261	12.363	10.475	1.767	1.979

Table 4
Estimation results of permeability of the unconventional sandstone reservoir of the "YANCHANG" formation in Xin'anbian area, Ordos Basin, China (five methods).

Sample number	*K* (This study)/10^{-3}μm^2	*K* (Yu & Li)/10^{-3}μm^2	*K* (Chen)/10^{-3}μm^2	*K* (Koponen)/10^{-3}μm^2	*K* (Plessis)/10^{-3}μm^2
A83-1	0.066	0.002	0.003	0.102	0.082
A83-2	0.029	0.000	0.001	0.044	0.035
A83-3	0.032	0.000	0.001	0.047	0.038
A83-4	0.075	0.003	0.004	0.115	0.092
A83-5	0.049	0.001	0.002	0.078	0.062
A83-6	0.075	0.003	0.004	0.116	0.092
A83-7	0.026	0.000	0.000	0.037	0.030
A83-8	0.016	0.000	0.000	0.024	0.019
A83-9	0.065	0.002	0.003	0.097	0.077
A83-10	0.058	0.002	0.003	0.094	0.075
A83-11	0.079	0.004	0.005	0.130	0.104
A83-12	0.031	0.000	0.001	0.050	0.040
A83-13	0.053	0.001	0.002	0.074	0.059
A83-14	0.055	0.001	0.002	0.086	0.068
A83-15	0.049	0.001	0.002	0.076	0.061
A83-16	0.044	0.001	0.001	0.071	0.057
A83-17	0.057	0.002	0.002	0.088	0.070
A83-18	0.050	0.001	0.001	0.073	0.058
A83-19	0.048	0.001	0.002	0.077	0.062
A83-20	0.070	0.003	0.004	0.110	0.088
A83-21	0.047	0.001	0.001	0.068	0.055
A83-22	0.055	0.001	0.002	0.083	0.067
A83-23	0.045	0.001	0.001	0.067	0.054
A83-24	0.042	0.001	0.001	0.069	0.055
A83-25	0.058	0.002	0.003	0.096	0.077
A83-26	0.061	0.002	0.002	0.092	0.074
A83-27	0.059	0.002	0.003	0.097	0.077
A83-28	0.046	0.001	0.002	0.072	0.058
A83-29	0.036	0.001	0.001	0.058	0.046
A83-30	0.062	0.002	0.003	0.097	0.077
A83-31	0.066	0.002	0.003	0.099	0.079
A83-32	0.052	0.001	0.002	0.086	0.069
A83-33	0.045	0.001	0.002	0.072	0.058
A83-34	0.047	0.001	0.001	0.072	0.057
A83-35	0.064	0.002	0.003	0.104	0.083

shows that when n is set to 1, the accuracy is the best that could also be proved by the following data. It is believed that the parameter "n" would be distinguished by the original properties of the reservoir.

In order to evaluate the accuracy and generalized performance of the five methods, including the "pore-throat divide-union" method, correlation analysis between permeability values in Table 4 and the porosity in Table 1 should be carried out. It was found to be characterized by the power function $K = ab^s$, as noted in Fig. 6 and Table 5.

The correlation coefficients R^2 of the five fitting equation in Table 5 are all above 0.95, which will be applied to the following accuracy and generalization performance test, so as to verify the superiority of the new theoretical estimation method.

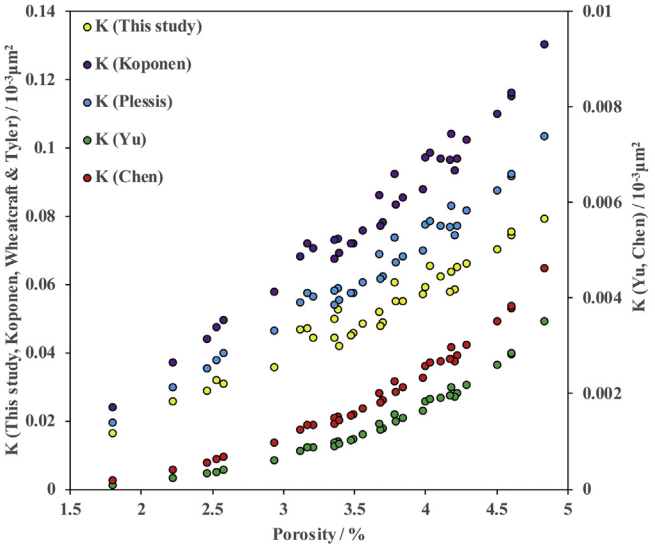

Fig. 6. Correlation of five types of permeability prediction value and porosity.

Table 5
Fitting constant of the power function in the correlation diagram of five types of permeability prediction value and porosity.

Permeability	Power function constant (a)	Power function index (b)	Correlation coefficient (R^2)
K (This study)/mD	0.0076	1.4879	0.9607
K (Yu & Li)/mD	0.00001	3.4827	0.9957
K (Chen)/mD	0.00004	3.0729	0.9947
K (Koponen/mD	0.0107	1.5612	0.9797
K (Plessis)/mD	0.0087	1.5487	0.9793

4. Case application

4.1. Rapid determination on absolute permeability of tight oil reservoir

The standard porosity and permeability test of the unconventional sandstone reservoir of the "YANCHANG" formation of Ordos Basin, China were carried out. The constants of five equations could be found in Table 5 so that we could generate permeability predictions of all samples, then compared the predicted results with measured results (Table 6), so as to verify the advantages and disadvantages of the five methods.

In order to prove the applicability and accuracy furtherly, some additional work should be carried out which is error analysis. First, the absolute values of the permeability differences between the measured values and the predicted values of the five methods should be

Table 6
Test and estimation results of permeability of the unconventional sandstone reservoir of the "YANCHANG" formation in the Xin'anbian area, Ordos Basin, China (five methods).

Sample number	Porosity/%	Permeability/$10^{-3}\mu m^2$	K (This study)/$10^{-3}\mu m^2$	K (Yu)/$10^{-3}\mu m^2$	*K* (Chen)/$10^{-3}\mu m^2$	*K* (Koponen)/$10^{-3}\mu m^2$	*K* (Plessis)/$10^{-3}\mu m^2$
A83-36	5.64	0.014	0.100	0.004	0.008	0.159	0.127
A83-37	4.76	0.034	0.077	0.002	0.005	0.122	0.097
A83-38	1.61	0.008	0.015	0.000	0.000	0.023	0.018
A83-39	1.41	0.006	0.013	0.000	0.000	0.018	0.015
A83-40	8.4	0.108	0.180	0.017	0.028	0.297	0.235
A83-41	8.5	0.153	0.184	0.017	0.029	0.302	0.239
A83-42	7.8	0.044	0.161	0.013	0.022	0.264	0.209
A83-43	7.83	0.051	0.162	0.013	0.022	0.266	0.211
A83-44	4.52	0.049	0.072	0.002	0.004	0.113	0.090
A83-45	4.87	0.049	0.080	0.002	0.005	0.127	0.101
A83-46	3.95	0.022	0.059	0.001	0.003	0.091	0.073
A83-47	4.04	0.031	0.061	0.001	0.003	0.095	0.076
A83-48	4.33	0.010	0.067	0.002	0.004	0.105	0.084
A83-49	12.42	0.459	0.323	0.065	0.092	0.546	0.431
A83-50	9.41	0.032	0.214	0.025	0.039	0.354	0.280
A83-51	4.84	0.038	0.079	0.002	0.005	0.125	0.100
A83-52	7.49	0.039	0.152	0.011	0.019	0.248	0.197
A83-53	9.25	0.260	0.208	0.023	0.037	0.345	0.273
A83-54	11.35	0.803	0.282	0.047	0.070	0.475	0.374
A83-55	8.62	0.096	0.187	0.018	0.030	0.309	0.245
A83-56	6.67	0.033	0.128	0.007	0.014	0.207	0.164
Average	6.56	0.111	0.134	0.013	0.021	0.219	0.173

calculated respectively. Second, the average of the above five absolute values were calculated. Third, the average of the predicted values and the measured values were also calculated. Finally, the absolute values of the permeability differences between the average measured values and the average predicted values of the five methods should be calculated respectively (Table 6). The accuracy and generalization performance could be reflected by the above parameters.

As can be seen in Fig. 7, the two errors of the pore-throat divide-union method are both the smallest, respectively $0.023 \times 10^{-3}\mu m^2$ and $0.090 \times 10^{-3}\mu m^2$; the average values of other four methods were $0.090 \times 10^{-3}\mu m^2$ and $0.108 \times 10^{-3}\mu m^2$, respectively. Thus, the new method described in this study demonstrates superiority and accurate generalization performance as regards estimation of pore-throat tortuosity and reservoir permeability combined with Kozeny-Carman equation.

Tight reservoirs and other tight oil reservoirs are different from conventional reservoirs because of their complex accumulation mechanisms and poor physical properties. Therefore, the permeability should be closely integrated with experiment and theory, so that they can be evaluated objectively and reasonably.

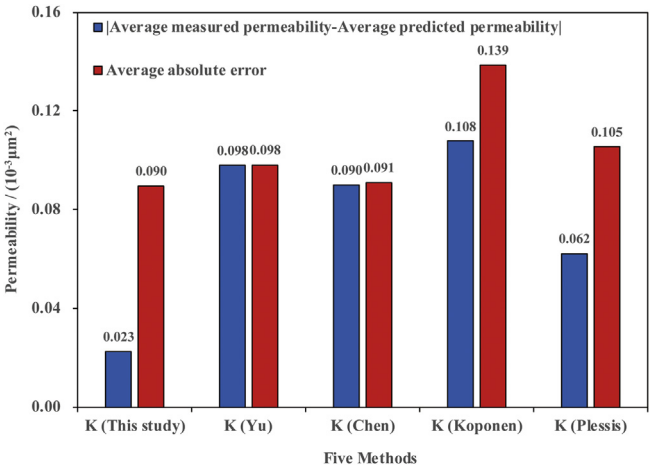

Fig. 7. Comparison of the methods' accuracy and generalization performance.

4.2. Quantitative determination of permeability anisotropy in tight oil reservoir

According to the requirement of "umbrella deconstruction" technology, field emission scanning electron microscopy (FIE-SEM) observation of reservoir slices in eight directions was carried out (Fig. 8). High-precision image processing was also carried out for reservoir imaging in eight directions by removing the invalid pore and throat. The dimensionless "n" in equation (4) is taken as 1, then the average radius, average length of major axis, average perimeter and pore-throat tortuosity were all calculated (Table 7). The permeability anisotropy can be quantitatively evaluated by plotting all the values into changing curves.

As can be seen from Fig. 9, the permeability curves of tight oil reservoir samples show that the permeability anisotropy of tight oil reservoir samples is remarkable. We could see that the sample has the highest permeability at the angle of 0°(180°/360°) and the permeability values are equal to $0.25 \times 10^{-3}\mu m^2$. Similarly, the sample has the lowest permeability at the angle of 22.5°(202.5°), 90°(270°), and 112.5°(292.5°), the permeability values are all equal to $0.06 \times 10^{-3}\mu m^2$. The extreme difference of permeability at different angles of the same sample (the ratio of maximum to minimum) could reach about 4, which fully proves that there are dominant permeability zones in tight oil reservoirs and this could not be ignored in the relative research in petroleum exploration and development.

5. Conclusion

Most of the current estimation methods of pore-throat tortuosity are focused on the testing of simplified models, and the majority of experimental and numerical simulation methods could only be used in reservoirs with high to moderate porosity and permeability. The method which originated from the original concept of pore-throat tortuosity is few. Thus, it does not meet the needs of permeability prediction in tight reservoirs; more accurate prediction ideas and means need to be discovered.

The significance of the minerals that grow in the particle boundary in the seepage process of the fluids should never be ignored. We should pay much more attention to this point when we investigate the precise method of permeability estimation of an unconventional reservoir.

The new permeability prediction model and its simplified form in

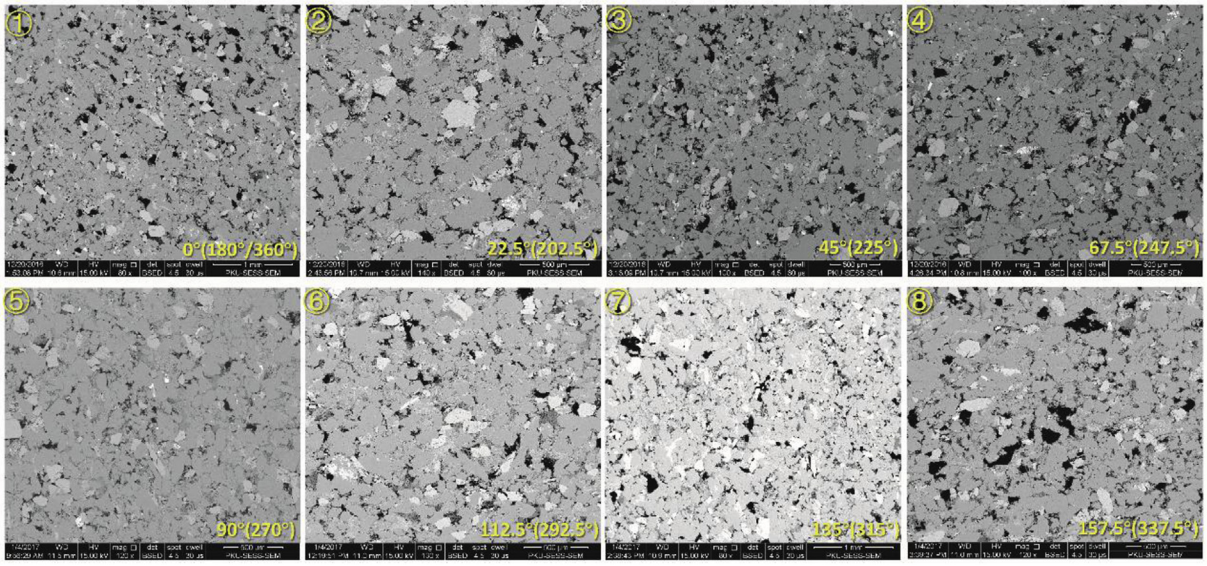

Fig. 8. High resolution FE-SEM images of tight oil reservoir samples using "Umbrella deconstruction" method (eight angels).

this study follows the original characteristics of the reservoir and then focuses closely on characteristics such as pore size and structure. In accordance with the principle of accurately describing the pore and throat in the full range, we calculated the pore-throat tortuosity of the unconventional reservoir under the multi-scale. The application in the unconventional sandstone reservoir of the "YANCHANG" formation in Xin'anbian area, Ordos Basin, China shows that the two errors of the new model which was proposed in this are the smallest of all methods examined so, combined with the Kozeny-Carman equation, the new method has demonstrated its superiority and robust generalization performance in estimating pore-throat tortuosity and reservoir permeability.

Finally, by combining the "umbrella deconstruction" method, we carry out the quantitative determination of permeability anisotropy in tight oil reservoir, which found that the permeability anisotropy of tight oil reservoir samples is very significant, and the extreme difference of permeability of the same sample at different angles (the ratio of maximum to minimum value) could reach 4. It fully proves that there are predominant permeability zones in tight oil reservoirs, which could not be ignored in petroleum research. The conclusions can provide important theoretical evidence and methodological basis for the process of oil filling and seepage recovery.

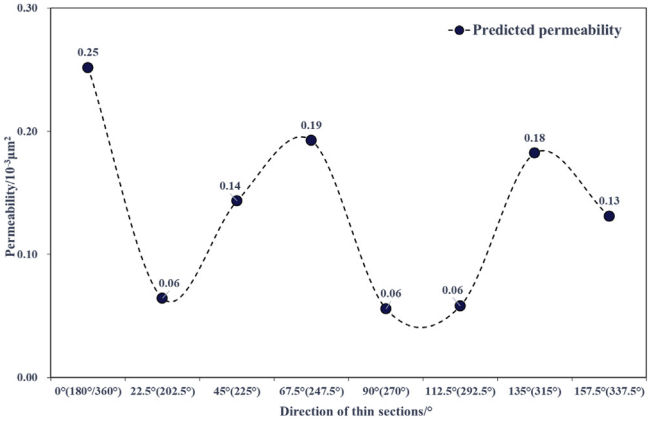

Fig. 9. The anisotropic permeability curve with the change of angles via precise pore-throat tortuosity characterization and "umbrella deconstruction" method.

Acknowledgement

This work is granted by open fund (No. PLC20190401) of state key laboratory of oil and gas reservoir geology and exploitation (Chengdu University of Technology) and the open fund project of the key Laboratory of Petroleum Resources Research, Institute of Geology and Geophysics, Chinese Academy of Sciences (No. KLOR2018-6). Thanks for the important support of Professor Yapu Zhao, Quanzi Yuan and Assistant Professor Xianfu Huang in Institute of Mechanics, Chinese Academy of Sciences.

Appendix A. Supplementary data

Supplementary data to this article can be found online at https://doi.org/10.1016/j.petrol.2019.03.009.

Table 7
Relative parameters of permeability calculation for tight oil reservoirs using "umbrella deconstruction" method and imaging processing.

Sampling angel	Sampling number	Pore radius/μm	Porosity/%	Perimeter/μm	Major axis/μm	Pore-throat tortuosity	Permeability/10^{-3}μm^2
0°(180°/360°)	1	7.79	11.21	43.50	12.89	3.38	0.25
22.5°(202.5°)	2	3.83	11.72	19.67	5.89	3.34	0.06
45°(225°)	3	5.55	12.80	30.51	8.86	3.44	0.14
67.5°(247.5°)	4	5.84	15.78	31.04	8.88	3.49	0.19
90°(270°)	5	4.34	7.75	25.03	7.65	3.27	0.06
112.5°(292.5°)	6	3.99	9.65	21.60	6.52	3.31	0.06
135°(315°)	7	7.28	8.95	40.20	12.37	3.25	0.18
157.5°(337.5°)	8	5.21	13.30	26.65	7.73	3.45	0.13

References

An, S.Y., Yao, J., Yang, Y.F., Zhang, L., 2016. Influence of pore structure parameters on flow characteristics based on a digital rock and the pore network model. J. Nat. Gas Sci. Eng. 31, 156–163.

Arash, Rabbani, Saeid, Jamshidi, Saeed, Salehi, et al., 2014. An automated simple algorithm for realistic pore network extraction from micro-tomography images. J. Pet. Sci. Eng. 123, 164–171.

Arash, Rabbani, Shahab, Ayatollahi, Riyaz, Kharrat, et al., 2016. Estimation of 3-D pore network coordination number of rocks from watershed segmentation of a single 2-D image. Adv. Water Resour. 94, 264–277.

Arash, Rabbani, Ali, Assadi, Riyaz, Kharrat, et al., 2017. Estimation of carbonates permeability using pore network parameters extracted from thin section images and comparison with experimental data. J. Nat. Gas Sci. Eng. 42, 85–98.

Beckingham, L.E., Peters, C.A., Um, W., et al., 2013. 2D and 3D imaging resolution tradeoffs in quantifying pore throats for prediction of permeability. Adv. Water Resour. 62, 1–12 Part A.

Boundreau, B.P., 1996. The diffusive tortuosity of finite - grained un-lithified sediments. Geochem. Cosmochim. Acta 60, 3139–3142.

Carman, P.C., 1939. Permeability of saturated sands, soils and clays. J. Agric. Sci. 29 (2), 263–273.

Chen, L., Gai, D., Sun, G., et al., 2011. A simple calculation method of pore and throat tortuosity. In: Proceedings of the Twentieth National Conference on Structural Engineering.

Comiti, J., Sabiri, N.E., Montillet, 2000. Experimental characterization of flow regimes in various porous media—III: limit of Darcy's or creeping flow regime for Newtonian and purely viscous non - Newtonian fluids. Chem. Eng. Sci. 55, 3057–3061.

Du, S., Pang, S., Shi, Y., 2018a. A new and more precise experiment method for characterizing the mineralogical heterogeneity of unconventional hydrocarbon reservoirs. Fuel 232, 666–671.

Du, S., Pang, S., Shi, Y., 2018b. Quantitative characterization on the microscopic pore heterogeneity of tight oil sandstone reservoir by considering both the resolution and representativeness. J. Pet. Sci. Eng. 169, 388–392.

Du, S., Shi, G., Shi, Y., et al., 2019. Imaging-based characterization of perthite in the upper triassic Yanchang formation tight sandstone of the Ordos Basin, China. Acta Geol. Sin.-Engl avaliable online in. https://doi.org/10.1111/1755-6724.13768.

Huang, X., Zhao, Y., 2017. Characterization of pore structure, gas adsorption, and spontaneous imbibition in shale gas reservoirs. J. Pet. Sci. Eng. 159, 197–204.

Kenneth, Chukwuma, Emese, M. Bordy, Angelique, Coetzer, et al., 2018. Evolution of porosity and pore geometry in the Permian Whitehill Formation of South Africa – a FE-SEM image analysis study. Mar. Petrol. Geol. 91, 262–278.

Kirill, M. Gerke, Roman, V. Vasilyev, Siarhei, Khirevich, et al., 2018. Finite-difference method Stokes solver (FDMSS) for 3D pore geometries: software development, validation and case studies. Comput. Geosci. 114, 1–58.

Koponen, A., Kataja, M., Timonen, J., 1996. Tortuous flow in porous media. Phys. Rev. E. 54, 406–410.

Kozeny, J., 1927. Ueber kapillare Leitung des Wassers im Boden. Sitzungsber Akad. Wins, Wien 136 (2a), 271–306.

Li, C., Zhang, X., 2007. Unification of flow equations in tubes and in porous media. Xinjiang Pet. Geol 28 (2), 252–253.

London, M., Cameron, S.M., Donald, J., Wassmuth, F.R., 2014. Water-flooding Experiments with X-Ray CT Imaging. Society of Petroleum Engineers.

Lonnes, S., Angel, G., Holland, R.N.M.R., 2003. Petrophysical predictions on cores. In: 44th Annual Logging Symposium Transactions. Society of Petroleum Well Log Analysts.

Lv, D., 2000. Calculation and application of hydraulics tortuosity factor in porous media. Xinjiang Pet. Geol. 21 (6), 515–517.

Nishank, Saxena, Ronny, Hofmann, Faruk, O. Alpak, 2017a. References and benchmarks for pore-scale flow simulated using micro-CT images of porous media and digital rocks. Adv. Water Resour. 109, 211–235.

Nishank, Saxena, Ronny, Hofmann, Faruk, O. Alpak, et al., 2017b. Effect of image segmentation & voxel size on micro-CT computed effective transport & elastic properties. Mar. Petrol. Geol. 86, 972–990.

Patrick, William, Michael, Corbett, Haitao, Wang, et al., 2017. Using the porosity exponent (m) and pore-scale resistivity modelling to understand pore fabric types in coquinas (Barremian-Aptian) of the Morro do Chaves Formation, NE Brazil. Mar. Petrol. Geol. 88, 628–647.

Plessis, J.P.D., Masliyah, J.H., 1988. Mathematical modelling of flow through consolidated isotropic porous media. Transport Porous Med 3 (2), 145–161.

Peng, R.D., Yang, Y.C., Ju, Y., et al., 2011. Computation of fractal dimension of rock pores based on gray CT images. Chin. Sci. Bull. 56, 3346.

Piela, K., Ooms, G., Sengers, J.V., 2009. Phenomenological description of phase inversion. Phys. Rev. 792 (Pt1), pp021403.

Rajkumar, K., Ramanathan, A.L., Behera, P.N., 2012. Characterization of clay minerals in the Sundarban mangroves river sediments by SEM/EDS. J. Geol. Soc. India 80, 429–434.

Ren, X.X., Li, A.F., He, B.Q., et al., 2015. Influence of the pore structures on stress sensitivity of tight sandstone reservoir. Adv. Petrol. Explor. Dev. 10, 13–18.

Rhiannon, T. Lewis, John, Georg Seland, et al., 2016. A multi-dimensional experiment for characterization of pore structure heterogeneity using NMR. J. Magn. Reson. 263, 19–32.

Rikan, Kareem, Pablo, Cubillas, Jon, Gluyas, et al., 2017. Multi-technique approach to the petrophysical characterization of Berea sandstone core plugs (Cleveland Quarries, USA). J. Pet. Sci. Eng. 149, 436–455.

Sen, P.N., Scala, C., Cohen, M.H., 1981. A self-similar model for sedimentary - rocks with application to the dielectric - constant of fused glass –beads. Geophysics 46, 781–795.

Shah, S.M., Gray, F., Crawshaw, J.P., et al., 2016. Micro-computed tomography pore-scale study of flow in porous media: effect of voxel resolution. Adv. Water Resour. 95, 276–287.

Song, W., Yao, J., Yang, L., et al., 2017. New pore size distribution calculation model based on chord length and digital image. J. Nat. Gas Sci. Eng. 48, 111–118.

Song, W.H., Yao, J., Ma, J.S., et al., 2018. Pore-scale numerical investigation into the impacts of the spatial and pore-size distributions of organic matter on shale gas flow and their implications on multiscale characterization. Fuel 216, 707–721.

Xiong, F., Jiang, Z., Zhang, L., 2016. The role of the residual bitumen in the gas storage capacity of mature lacustrine shale: a case study of the Triassic Yanchang shale, Ordos Basin, China. Mar. Petrol. Geol. 69, 205–215.

Yang, Y.F., Zhang, W.J., Gao, Y., et al., 2016. Influence of stress sensitivity on microscopic pore structure and fluid flow in porous media. J. Nat. Gas Sci. Eng. 36, 20–31 Part A.

Yang, X., Meng, Y., Shi, X., et al., 2017. Influence of porosity and permeability heterogeneity on liquid invasion in tight gas reservoirs. J. Nat. Gas Sci. Eng. 37, 169–177.

Yu, B.M, Li, J.H., Li, Z.H., Zou, M.Q., 2003. Permeabilities of unsaturated fractal porous media. Int. J. Multiph. Flow 29, 1625–1642.